Improving the Mismatch between Light and Nanoscale Objects with Gold Bowtie Nanoantennas

P. J. Schuck,[1] D. P. Fromm,[1] A. Sundaramurthy,[2] G. S. Kino,[2] and W. E. Moerner[1]
[1]*Department of Chemistry, Stanford University, Stanford, California 94305, USA*
[2]*Department of Electrical Engineering, Stanford University, Stanford, California 94305, USA*
(Received 16 September 2004; published 13 January 2005)

Metallic bowtie nanoantennas should provide optical fields that are confined to spatial scales far below the diffraction limit. To improve the mismatch between optical wavelengths and nanoscale objects, we have lithographically fabricated Au bowties with lengths ~75 nm and gaps of tens of nm. Using two-photon-excited photoluminescence of Au, the local intensity enhancement factor relative to that for the incident diffraction-limited beam has been experimentally determined for the first time. Enhancements $>10^3$ occur for 20 nm gap bowties, in good agreement with theoretical simulations.

DOI: 10.1103/PhysRevLett.94.017402 PACS numbers: 78.67.–n, 33.80.–b, 42.30.–d, 42.50.Hz

In recent years, a variety of schemes have been explored to improve the mismatch between typical optical wavelengths (hundreds of nm) and much smaller nanoscale objects. For example, excitation of surface charge or plasmons in sharp tips produces enhanced optical fields confined locally to regions approximately equal in size to the radius of curvature of the tip (~10 nm) [1–4]. Near-field intensity (I) enhancements for Au tips are predicted to be as large as 10^3 under optimal conditions [1], and enhancements of roughly 50 times (in I) have been measured experimentally [2]. In the related field of surface enhanced Raman scattering (SERS), even larger electromagnetic (as opposed to ''chemical'') enhancements up to 10^6 in I are at least partially responsible for the detection of single-molecule Raman spectra [5,6]. Investigators have suggested that these ultraintense fields are created by strong plasmonic coupling between pairs of small metallic spheres [6–8]. However, all single-molecule SERS studies to date have used randomly deposited colloidal particles, leading to increased interest in the design and characterization of coupled nanoparticles that can be reproducibly fabricated. Subwavelength-sized lithographic metallic particles have been investigated for both arrays of particles [9,10], single particle pairs [11,12], and metallic shells [13]. While various calculations suggest large enhancements can occur, experimental values for optical field enhancement have yet to be directly measured.

''Bowtie'' antennas, consisting of two metallic triangles facing tip to tip that are separated by a small gap, combine the electromagnetic properties of sharp metal tips with those of coupled plasmon resonant nanoparticle pairs. Bowties were first proposed in the microwave regime [14], and various antennas have been studied at midinfrared wavelengths near 10 μm [15]. Recently, we have fabricated Au bowtie antennas for use in the visible by e-beam lithography, and the scattering resonance behavior as a function of gap size for single bowties has been measured [12] and compared with finite-difference time-domain (FDTD) calculations using the required wavelength-dependent dielectric functions [16]. These calculations also predict an intensity enhancement factor in the gap in excess of 1500. In this Letter, we present experimentally determined optical intensity enhancement values for the fields *in the metal* of these structures, which closely approximate fields just outside the metal, near the surface.

Strongly enhanced local fields due to the excitation of surface plasmons in rough films, sharp tips, and nanoparticles give rise to detectable two-photon absorption in Au [17–19]. The resulting excitation of electrons from the d valence band to the sp conduction band leads to a broadband emission continuum, termed two-photon excited photoluminescence (TPPL) in Au [18–20]. Because of its nonlinear dependence on excitation intensity, TPPL is a sensitive probe of excitation field strength and distribution. Here, we use TPPL to directly determine absolute values for optical field enhancements of single Au bowties by comparing the strength of TPPL from bowties with TPPL from a smooth Au film.

Au bowties were fabricated with electron beam lithography on a fused silica cover slip as previously described [12]. Each triangle of a bowtie was 75 ± 5 nm in length, had a tip radius of curvature of 18 ± 2 nm, an Au thickness of ~18 nm, and a 3.0 nm Ti adhesion sticking layer. The sample consisted of multiple bowtie arrays, with varying gap size, and a 3 μm spacing between bowties. Au squares, $8\ \mu\text{m} \times 8\ \mu\text{m}$ in size and ~38 nm thick, provided calibration regions. Average surface roughness for both the bowties and the squares was 2.5 nm rms measured with atomic force microscopy (AFM).

TPPL was measured with a sample-scanning inverted optical microscope. A mode-locked Ti:sapphire laser ($\tau =$ 120 fs, $f = 75$ MHz, $\lambda = 830$ nm) was used for excitation. The value $\lambda = 830$ nm was chosen since the smallest gap bowties were measured [12] to be resonant at this wavelength. The laser is focused to a diffraction-limited spot on the bowtie-air interface using a 1.4 numerical aperture (N.A.), 100× oil objective. Au TPPL is collected by the same objective and passed through spectral filters that transmit only wavelengths between 460 and 700 nm. The luminescence is focused onto a single-photon counting avalanche photodiode (APD) for broadband collection. After optical experiments, the sample is studied with an

AFM, then coated with a thin Cr layer (~4 nm) for particle analysis in the scanning electron microscope (SEM) to carefully measure gap sizes. The TPPL spectrum from a single bowtie matches the broadband continuum emission of Au TPPL [18,19].

Figure 1(c) shows a 23 μm by 23 μm TPPL image for bowties with nominal gap sizes of 20 nm, excited by an incident polarization parallel to the bowtie axis. Approximately 50% of the bowties in this array emit a detectable amount of TPPL, and there is a large variation in observed intensities. Nevertheless, the array periodicity of 3 μm $\times$ 3 μm is clearly visible, evidence the emission originates from the bowties. The variation in TPPL brightness is, in general, *not* due to local film roughness, but is a consequence of the different gap sizes present in this array. Though all bowties within this array were designed to have 20 nm gaps, actual gap sizes range from 0 to 28 nm as later determined by SEM. A distribution of gap sizes is expected since feature dimensions on the order of 15 nm are near the limits of the fabrication procedure, which was optimized to give a range of gap sizes rather than highly reproducible bowties of the smallest gap. All ''dark'' bowties in the image (bowties with TPPL below the noise floor of our detector) were shown by SEM to have a gap size below the SEM resolution; i.e., the triangles were likely touching, or ''shorted.'' It is also possible that some bowties which appear shorted via SEM may have very small gaps; the resulting extremely redshifted resonance wavelength [12] would make these difficult to pump.

The TPPL signals from this array exhibited a strong dependence on incident polarization, evidence that the TPPL is a result of field enhancement due to triangle-triangle coupling within each bowtie and not from ''hot spots'' of uncontrolled position. An example is shown for a typical 20 nm gap bowtie [Figs. 1(a) and 1(b)], where the integrated TPPL intensity for hot axis excitation is 166 times greater than for perpendicular polarization.

A 23 μm by 23 μm TPPL image of a bowtie array with nominal gaps of 400 nm is shown in Fig. 1(d). This image was acquired using an average pump power 10 times higher than that for Fig. 1(c). TPPL is detected at all bowties, but without polarization dependence. Also, the two constituent triangles of each bowtie can be clearly resolved, and the TPPL intensities from the two triangles often differ. These observations demonstrate that only minimal, if any, electromagnetic coupling exists between triangles in a given bowtie at this large gap; i.e., each triangle behaves similarly to an isolated Au triangle [12,16]. Field enhancement is still expected from single metallic triangles due to their sharp tips, but to a much lesser degree than that from coupled pairs.

To directly determine optical field enhancements from bowtie nanoantennas, the TPPL properties of smooth Au films were measured as a calibration. Figure 1(e) is a TPPL image from an Au film square. TPPL is brightest at the edges due to the field enhancement caused by localized plasmon resonances at the rough edge, which result from the lift-off procedure [18,19]. Less intense and remarkably uniform TPPL is also observed from the interior of the square. Five hot spots of localized field enhancement are also visible, or less than one hot spot per 10 μm^2, providing optical evidence of the film's smoothness. The APD signal from the uniform luminescence regions (regions containing no TPPL hot spots) was 18 $\pm$ 4.3 counts/10 ms after subtraction of detector dark counts.

The TPPL intensity dependence is shown in Fig. 2 for a smooth Au film, a single 400 nm gap bowtie, and a single bowtie from the array with nominal gap size of 20 nm. APD count rates from the Au film were normalized for the relative surface area of Au illuminated by the focused laser. For the Au film and 400 nm gap bowtie, the collected emission shows a quadratic dependence for all intensities studied, as expected for TPPL. For the bowtie from the 20 nm gap array, the TPPL follows a quadratic dependence at low average powers. As incident power increases, however, TPPL intensity deviates from this dependence until, at still higher powers, it again shows a quadratic dependence but along an I^2 curve shifted to the right of the

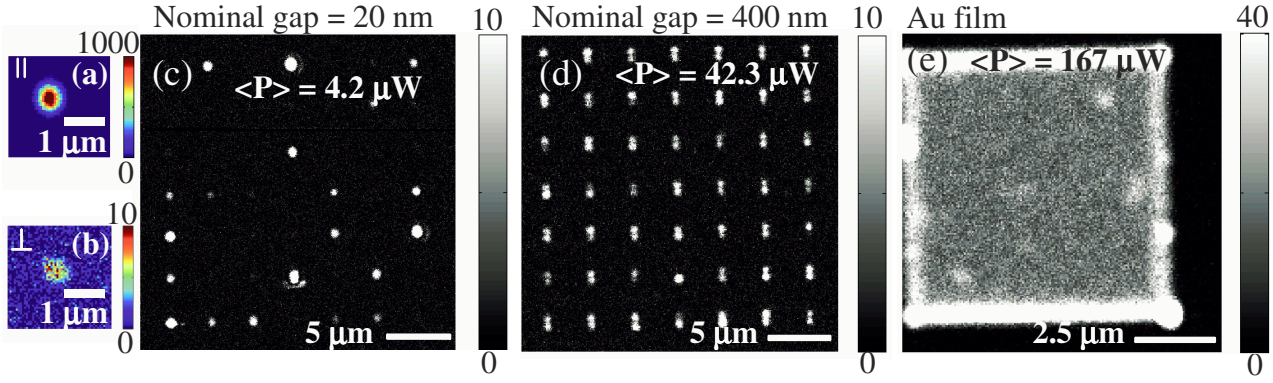

FIG. 1 (color online). Visible luminescence images from bowtie arrays with nominal gap sizes of 20 nm (c) and 400 nm (d), as well from a smooth Au film (e), with 10 ms per pixel, 830 nm pump, and average incident powers (c) 4.2 μW, (d) 42.3 μW, (e) 167 μW. Strong TPPL originates from the edges of the film in (e) due to increased surface roughness resulting from the lift-off procedure. Incident polarization dependence is shown in (a) and (b) for a 20 nm gap bowtie at high power (note different scales).

original curve. This behavior occurs for almost all small gap bowties (gaps <40 nm) and is interpreted as follows: At low powers, the bowtie is exposed to a near-field intensity equal to the incident intensity times the intensity enhancement factor of the bowtie. Eventually, the field intensity becomes large enough to physically damage the bowtie, causing an emission decrease. In this context, damage is defined as any irreversible change to the particle that reduces its field-enhancing capabilities. The deviation from an I^2 dependence continues until the damage-induced change reduces the enhancement factor to a value such that the enhanced field is well below the damage threshold. Thereafter, the emission follows a new quadratic curve defined by the lower enhancement factor. For subsequent measurements at low powers, the measured TPPL lies on the shifted curve (open square in Fig. 2), indicating an irreversible change. Note that the original gap size for this particle is not known since it was damaged before SEM analysis; thus we use the phrase "nominal gap size of 20 nm."

If one makes the assumption that no field enhancement occurs in a smooth film, then an intensity enhancement in the metal of bowtie i, α_{bt}^{i}, can be calculated from the ratio of TPPL intensities from the bowtie and the film. This ratio is given by

$$\frac{\langle \mathrm{TPPL}_{bt}^{i} \rangle}{\langle \mathrm{TPPL}_{\mathrm{film}} \rangle} = \frac{A_{bt}}{A_{\mathrm{film}}} \frac{(\alpha_{bt}^{i})^2 \langle P_{bt}^{i} \rangle^2}{\langle P_{\mathrm{film}} \rangle^2}, \tag{1}$$

where $\langle \mathrm{TPPL}_{bt}^{i} \rangle$ is the (time averaged) TPPL signal when bowtie i is centered in the focus of the laser excitation spot measured by determining the peak of a Gaussian fit to the spot in images like Fig. 1(c), $\langle \mathrm{TPPL}_{\mathrm{film}} \rangle$ is the TPPL signal when the spot is anywhere within the uniform emission from the Au film, $\langle P_{bt}^{i} \rangle$ is the average incident power at bowtie i that yields $\langle \mathrm{TPPL}_{bt}^{i} \rangle$, $\langle P_{\mathrm{film}} \rangle$ is the average incident power at the film that yields $\langle \mathrm{TPPL}_{\mathrm{film}} \rangle$, A_{bt} is the surface area of the bowtie from which the $\langle \mathrm{TPPL}_{bt}^{i} \rangle$ originates, and

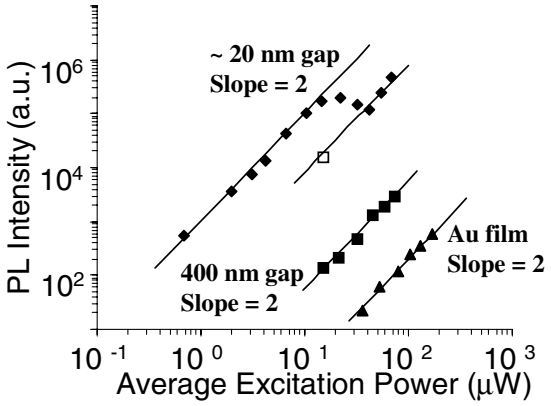

FIG. 2. TPPL intensity dependences for a smooth Au film, a 400 nm gap bowtie, and a bowtie from an array with nominal gap size of 20 nm. Open square: measurement at a lower power after the intensity scan.

A_{film} is the total surface area of the Au film from which the $\langle \mathrm{TPPL}_{\mathrm{film}} \rangle$ originates. Following [21], we assume the area A_{film} excited by two-photon absorption of the focused laser is equal to a circular region with a diameter equal to the full width at half maximum (FWHM) of the appropriate objective response function, here the square of the intensity point spread function of our microscope objective. For $\lambda =$ 830 nm and N.A. = 1.4, the measured FWHM from a diffraction-limited TPPL spot is equal to 214 nm, so $A_{\mathrm{film}} = 35\,600\ \mathrm{nm}^2$. FDTD calculations show that plasmonic current densities and optical near-field intensities are concentrated in a confined region of each bowtie, e.g., within the Au nearest the gap, particularly for bowties with small gap sizes; thus A_{bt} is also gap dependent and must be calculated.

Previous FDTD computations of Au bowtie nanoantenna properties exhibit excellent agreement with experimental values [12,15,16]. The earlier studies showed that the strongest optical fields are in the center of the gap between the triangles. However, the experimentally observed TPPL certainly arises from electromagnetic fields *in the metal.* Therefore, the TPPL intensity should be proportional to the fourth power of electric field in the metal, E_m, and the total TPPL power will be correlated to the integral of $|E_m|^4$.

Plane wave excitation normally incident on the bowties is assumed in the FDTD calculations. For electric field amplitude E_0, the tangential electric field at the metal surface is E_{inc} where $E_{\mathrm{inc}} = 2E_0/[1 + (n + jk)]$ and $(n + jk)$ is the complex refractive index of the metal [22]. In the Au film, the electric field falls off as $\exp(-kz)$. FDTD simulations show that, to good approximation, the E field in the bowties also falls off as $\exp(-kz)$. Since all fields have the same z dependence in the metal, the integral of $|E_m|^4$ need be performed only along the x and y directions just below the surface of the metal in the FDTD computations so as to yield results comparable to experiment.

We use FDTD calculations to determine the square of the intensity enhancement in bowtie i, $|\alpha_{bt}^{i,\mathrm{FDTD}}|^2$:

$$|\alpha_{bt}^{i,\mathrm{FDTD}}|^2 = \frac{\iint |E_{bt,m}|^4 dxdy}{\iint E_{\mathrm{incident}}^4 dxdy},$$

where $|E_{bt,m}|^4 = (E_{bt,mx}^2 + E_{bt,my}^2 + E_{bt,mz}^2)^2$ and the integral is over the x and y dimensions of the bowtie. The experimental and theoretical results for $|\alpha_{bt}^{i}|^2$ are shown in Fig. 3 for various gap widths. The effective area A_{bt} of the TPPL source is determined from the following integral:

$$A_{bt} = \int E_m^4 dxdy / E_{\mathrm{max}}^4,$$

where E_{max} is the maximum field in the bowtie. A_{bt} is a function of gap size, increasing as gap width increases. The theoretical A_{bt} for the smallest gap width (16 nm) was 642 nm^2, indicating the field was confined to approximately one-tenth of the ~6530 nm^2 area of the bowtie. Using these values for A_{bt} in Eq. (1) along with the

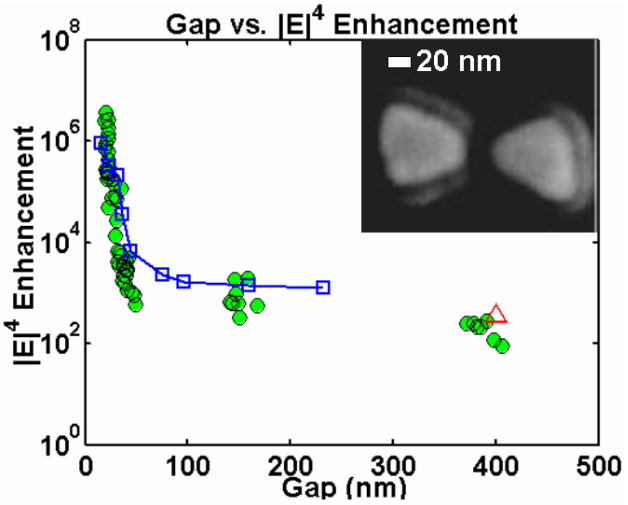

FIG. 3 (color online). Comparison of experimental (circles) and theoretical (open squares) values of the square of intensity enhancement, $(\alpha_{bt}^{i})^2$, for bowties with gaps of 16 to 406 nm. FDTD simulations for $(\alpha_{bt}^{i})^2$ at an individual triangle are used for comparison to the bowties with nominal gap size of 400 nm. Excellent agreement is observed, especially for the largest and smallest gap sizes where experimental conditions most closely approximate the theoretical treatment. Inset: SEM image of a representative bowtie, gap size = 22 nm. The "halos" surrounding each triangle are due to charging effects and are not real.

experimentally determined TPPL intensities yields E^2 enhancement factors $>10^3$ ($>10^6$ for α^2) for bowties with the smallest gaps. These are the largest such factors reported to date for lithographically produced nanoantennas. We observe good agreement between the E^4 values for theory and experiment for gap widths less than 30 nm, but slightly less so for gap widths of 40–60 nm. For nominal gap widths of 400 nm, we again get good agreement. This can be explained by the fact that the plane wave excitation used for FDTD closely approximates the experimental conditions for small gap bowties, but does not accurately model intermediate gaps, where the triangles are not uniformly pumped by the focused laser spot. To avoid this difficulty for gap widths of 400 nm, we excited and collected TPPL from each triangle of the bowtie separately and summed the two since the coupling is minimal. Furthermore, since a 400 nm gap bowtie was too large to simulate, the FDTD E^4 enhancement value was obtained by doubling the value from simulations for a single triangle (Fig. 3, triangle).

A strong lower bound on field enhancement in the metal for a bowtie follows by assuming the *entire* bowtie is exposed to the enhanced field and generates TPPL, i.e., $A_{bt} = 6530$ nm^2. Even with this conservative assumption, intensity enhancements are still >650 for bowties with 20 nm gaps. Ultimately, the fields outside the metal in the gap are of primary interest in many spectrosopic contexts. Our determination of the field in the metal is a good estimate of the field in the gap: for a 16 nm gap bowtie pumped at $\lambda = 830$ nm, FDTD predicts an intensity enhancement factor of $\sim$1000 just inside the metal (Fig. 3) and $\sim$1500 in the gap, 4 nm from the bowtie's surface.

In conclusion, we have experimentally measured optical intensity enhancements at lithographically produced Au bowtie nanoantennas of various gap sizes using TPPL, and find good agreement with FDTD simulations. For small gap bowties, the field enhancement is $>10^3$ confined to a region $\sim$650 nm^2, which may be interpreted as a dramatic improvement in the mismatch between conventional optical excitations and nanoscale structures. The large enhanced fields in the metal will also lead to similarly enhanced, localized fields on the metallic surface and in between the two bowties. This will yield extremely intense near-field optical light sources with high local contrast that have applications ranging from the elucidation of SERS mechanisms, ultrasensitive biological detection, and nanometer-scale lithography to high-resolution optical microscopy and spectroscopy.

D. F. thanks the National Science Foundation. This work was supported in part by the National Institutes of Health Grant No. 1R21-GM065331 and the Department of Energy Grant No. DE-FG03-00ER45815.

[1] E. J. Sanchez, L. Novotny, and X. S. Xie, Phys. Rev. Lett. **82**, 4014 (1999).
[2] A. Hartschuh *et al.*, Phys. Rev. Lett. **90**, 095503 (2003).
[3] A. Hartschuh *et al.*, Science **301**, 1354 (2003).
[4] H. F. Hamann *et al.*, J. Chem. Phys. **114**, 8596 (2001).
[5] S. Nie and S. R. Emory, Science **275**, 1102 (1997).
[6] K. Kneipp *et al.*, J. Phys. Condens. Matter **14**, R597 (2002).
[7] H. Xu *et al.*, Phys. Rev. Lett. **83**, 4357 (1999).
[8] A. M. Michaels, J. Jiang, and L. Brus, J. Phys. Chem. B **104**, 11 965 (2000).
[9] C. L. Haynes *et al.*, J. Phys. Chem. B **107**, 7337 (2003).
[10] W. Rechberger *et al.*, Opt. Commun. **220**, 137 (2003).
[11] K. H. Su *et al.*, Nano Lett. **3**, 1087 (2003).
[12] D. P. Fromm *et al.*, Nano Lett. **4**, 957 (2004).
[13] J. B. Jackson *et al.*, Appl. Phys. Lett. **82**, 257 (2003).
[14] R. D. Grober, R. J. Schoelkopf, and D. E. Prober, Appl. Phys. Lett. **70**, 1354 (1997).
[15] K. B. Crozier *et al.*, J. Appl. Phys. **94**, 4632 (2003).
[16] A. Sundaramurthy (private communication).
[17] C. K. Chen, A. R. B. de Castro, and Y. R. Shen, Phys. Rev. Lett. **46**, 145 (1981).
[18] G. T. Boyd, Z. H. Yu, and Y. R. Shen, Phys. Rev. B **33**, 7923 (1986).
[19] M. R. Beversluis, A. Bouhelier, and L. Novotny, Phys. Rev. B **68**, 115433 (2003).
[20] A. Bouhelier, M. R. Beversluis, and L. Novotny, Appl. Phys. Lett. **83**, 5041 (2003).
[21] A. Hartschuh *et al.*, Philos. Trans. R. Soc. London A **362**, 807 (2004).
[22] E. D. Palik, *Handbook of Optical Constants* (Academic Press, Orlando, 1985).